Energy-Efficient Array Transmitters Through Outphasing and Over-the-Air Combining

Vesa Lampu*, Guixian Xu*, Lauri Anttila*, Alberto Brihuega*, Marko Kosunen†,
Vishnu Unnikrishnan*, Jussi Ryynänen†, and Mikko Valkama*
*Department of Electrical Engineering, Tampere University, 33720 Tampere, Finland
†Department of Electronics and Nanoengineering, Aalto University, 02150 Espoo, Finland
E-mail: vesa.lampu@tuni.fi

***Abstract*—In this paper, a combinerless outphasing architecture for multiantenna transmitters with analog beamforming is presented and analyzed. The outphasing transmitter facilitates the use of highly power efficient switch-mode power amplifiers (PAs), while the combinerless structure further simplifies and improves the power efficiency of the design. The combining of the component outphasing signals in such a system then occurs over-the-air, at the receiver antenna. We consider two cases, one where the transmit outphased signals are alternately fed to the individual antennas and another where they are grouped in subarrays, and derive the analytical expressions for the total power beampatterns in both cases. Additionally, we carry out extensive simulations to verify the beampattern results and to evaluate the inband and out-of-band emission characteristics of the system, in terms of error vector magnitude (EVM) and total radiated power (TRP)-based adjacent channel leakage ratio (ACLR). We also consider these metrics under gain and phase mismatches in the transmitting antenna branches. The simulation results indicate that the system is able to attain good EVM results, while also the TRP-based ACLR limits imposed by 3GPP can be met if substantially large number of antennas are employed.**

***Index Terms*—Outphasing, Antenna arrays, Analog beamforming, Beampattern, Receiver combining**

I. Introduction

The large-scale adoption of the use of massive multiple-input multiple-output (MIMO) techniques, which utilize up to thousands of antennas, significantly increases the power consumption of the transmitters. It is therefore imperative for the next generation of radio transmitter systems to be as energy efficient as possible, while retaining high-level Quality of Service (QoS) and coverage [1]. Furthermore, to ensure cost-effectiveness, the systems have to be manufactured using cheap components, which tend to suffer from considerable non-idealities. Thus, simplifying the transmitter implementation and compensating for the non-ideal characteristics of the cheap components are very important research topics.

Recent developments tackling the aforementioned issues in the MIMO and large antenna array contexts are abundant in literature. One proposed solution is to reduce the quantization accuracy (i.e., the bits) of the digital-to-analog converter (DAC) of the transmitter, which is one of the pivotal power draining parts of the system, thus reducing the total power consumption of the transmitter [2]. The other major power drain in the circuits is the radio frequency (RF) power amplifier (PA). Besides draining a lot of power, the PAs, especially low-cost ones, exhibit strongly nonlinear behaviour in the presence of high peak-to-average power (PAPR) signals, which modern waveforms, such as the orthogonal frequency-division multiplexing (OFDM), tend to have. A possible way to mitigate this effect is to reduce the transmit signal power, i.e., back-off the PA, which debases the already poor power efficiency even further. A widely studied solution to this issue is the use of digital predistortion (DPD) [3], [4], which linearizes the PA output, thus allowing the PAs to function near the maximum possible efficiency. Another way around the PA nonlinearity issue is to utilize constant envelope (CE) waveforms [5], [6], which do not excite spectral regrowth in the PA, only harmonics. Furthermore, the use of CE signals enables the adoption of switch-mode PAs (e.g., class-E), which operate more efficiently than their more widely-used class-B or class-AB counterparts.

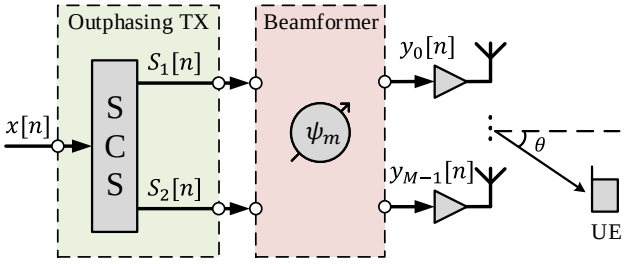

Fig. 1. Considered transmitter system baseband model, consisting of a single outphasing transmitter and a beamformer, serving M total antennas.

In this paper, we consider an outphasing transmitter [7], [8] structure to improve the energy efficiency of the transmitter. The outphasing transmitter divides the transmit signal into two component signals, which are CE waveforms. Therefore, amplifying these signals does not cause spectral regrowth, and can be carried out in a switch-mode PA, increasing the power efficiency. Due to the switching operation, the outphasing transmitter is a favorable option for higher frequency operation [9], such as for the frequency range (FR)-2 introduced in the 3GPP 5G NR specifications [10]. Our modeling specifically aims towards the FR-2 range, where the channels are dominated by the line-of-sight (LOS) components.

In a conventional outphasing transmitter architecture, the outphasing component signals are combined after the PA, to produce an amplified version of the original signal, which is consequently transmitted. In this paper, the design is simplified

by omitting the combining of the signals, and we let the signals combine over-the-air (OTA) at the intended receiver. This combinerless outphasing has been studied previously e.g., in [11]–[14], with moderate amount of transmitting antennas. More recently, [15] covered a case with multiple transmitting antennas and a functioning prototype.

The aim of this paper is to further study the combinerless outphasing in an antenna array context and perform initial verification of the feasibility of the scheme as a potential substitute for the Cartesian architecture. The contributions and novelties are as follows. We investigate the total power emissions of the combinerless outphasing structure by deriving and simulating the total power beampatterns for two distinct cases. Additionally, the inband and out-of-band (OOB) emission levels are studied through simulations. We also consider the signal quality aspects through error vector magnitude (EVM) and total radiated power (TRP)-based adjacent channel leakage ratio (ACLR). These metrics are further evaluated within a system, where the antenna branches suffer from unbalanced gain and phase. Comparing the aforementioned issues with the Cartesian architecture equivalents gives insight whether the outphasing structure is a valid substitute as is, or if further innovations are required.

The rest of the paper is organized as follows. Section II defines the overall system model, including the outphasing transmitter, beamforming and receiver combining. In Section III, two distinct beamforming cases are presented and their total power beampattern expressions are derived. Section IV shows simulation results with the derived beampatterns, and signal quality metrics of EVM and TRP-based ACLR in various settings. Finally, Section V concludes the paper.

II. System Model

We consider a high frequency point-to-point system, consisting of an M antenna array (M being even) outphasing transmitter and a single antenna receiver, as depicted in Fig. 1. The outphasing transmitter will produce the transmitted signals for the antenna array. Then, the beamformed signals propagate through a wireless channel, after which they are coherently combined at the receiver. In a standard outphasing transmitter, the outphased component signals would be combined after amplification, to produce a new amplified version of the original signal, which would then be transmitted. In this paper, however, we consider no summation of the outphasing signals at the transmitter side, and instead opt to transmit the component signals as is, and let them combine OTA at the receiver.

A. Outphasing Transmitter

The input signal $x[n]$ can be defined as a generic complex valued baseband signal by the expression

$$x[n] = A[n]\exp(j\phi[n]), \tag{1}$$

where $A[n]$ and $\phi[n]$ denote the amplitude and the phase of the signal, respectively and n is the discrete time index. For simplicity, we consider the amplitude normalized, i.e., $A_{\max} = 1$. Additionally, we assume the signal $x[n]$ to be zero-mean and the real and imaginary parts to be independent and identically distributed (i.i.d.).

The outphasing scheme takes advantage of the decomposition of a signal to two CE ones [16], [17]. The signal component separator (SCS) produces these outphasing signals $S_1[n]$ and $S_2[n]$, defined as

$$S_1[n] = x[n] + e[n], \tag{2}$$
$$S_2[n] = x[n] - e[n], \tag{3}$$

where $e[n]$ is given by

$$e[n] = jx[n]\sqrt{\frac{A_{\max}^2}{A[n]^2} - 1}. \tag{4}$$

By substituting (1) and (4) to both (2) and (3) and by noting the amplitude normalization, after some simple arithmetic, we have

$$S_1[n] = A[n]\exp(j\phi[n]) + \sqrt{1 - A[n]^2}\exp(j(\phi[n] + \frac{\pi}{2})), \tag{5}$$

$$S_2[n] = A[n]\exp(j\phi[n]) + \sqrt{1 - A[n]^2}\exp(j(\phi[n] - \frac{\pi}{2})). \tag{6}$$

The outphased component signals $S_1[n]$ and $S_2[n]$ are now CE signals, which means they can be amplified in highly nonlinear PAs without the nonlinear distortion compromising the signal quality, and efficient switch-mode PAs can be used as well [9].

B. Beamformer

In this work, we consider a uniform linear array (ULA) type of antenna group. For analytical simplicity, the antennas are assumed perfect isotropic antennas and the system is assumed to be narrowband. Hence, the beamforming can be carried out simply by phase shifting the consecutive antenna signals by

$$\psi_m = 2\pi m\frac{d\sin(\theta)}{\lambda} = 2\pi m\rho\sin(\theta), \tag{7}$$

where ψ_m is the phase shift to be applied, $m \in \{0, 1, \cdots, M-1\}$ the antenna index, d the antenna separation, θ the angle of the intended user from the array norm, as depicted in Fig. 1, λ the wavelength of the transmitted signal and $\rho = d/\lambda$ the ratio of antenna separation and wavelength. Now, using (5), (6) and (7), we can define the transmitted signal $y_m[n]$ at antenna indexed m as

$$y_m[n] = \exp(-j\psi_m)S_{1,2}[n], \tag{8}$$

where $S_{1,2}[n]$ is either $S_1[n]$ or $S_2[n]$, selected based on the configuration of the system and the antenna index, explained in detail in Section III. For the modeling purposes, we omit the PA gain, as it only scales the signals up due to the lack of produced nonlinear distortion.

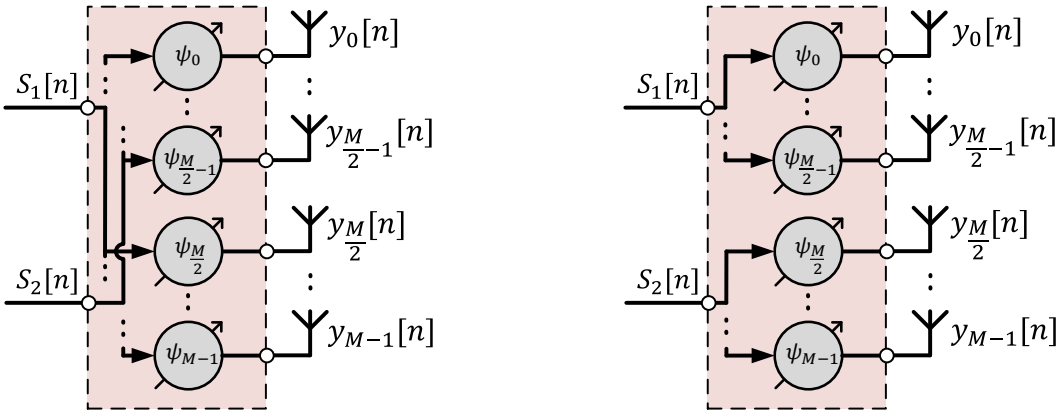

(a) (b)

Fig. 2. Considered beamforming schemes, with (a) corresponding to alternating signal scheme, and (b) to block-based scheme.

C. Channel and Receiver Combining

Assuming that the system is operated at millimeter wave (mmWave) frequencies, we consider a non-fading, multipath-free LOS channel, where the signals are simply phase rotated based on the angle of investigation θ' and the antenna index. The phase rotation a for a signal propagating from antenna indexed m towards angle θ' is defined then as

$$a_{m,\theta'} = 2\pi m\rho \sin(\theta'). \tag{9}$$

Finally, the received signal $r[n,\theta]$ at angle θ' is the superposition of all transmitted signals, written as

$$r[n,\theta'] = \sum_{m=0}^{M-1} \exp(ja_{m,\theta'})y_m[n]. \tag{10}$$

For simplicity, we omit the noise in the system from our models. It is worth noting, that at the intended angle ($\theta' = \theta$), the received signal in (10) reduces to

$$r[n,\theta] = Mx[n], \tag{11}$$

indicating that the signals combine perfectly to produce the transmitted signal at this angle.

III. Beamforming Schemes and Beampattern Derivations

In this Section, we develop models for the received total radiated power beampatterns, in order to study the feasibility of two basic arrangements of the transmitted outphasing signals. The considered signal configurations are depicted in Fig. 2, which will be explained in the following subsections. For both cases, we will utilize the same SCS and basic beamforming schemes introduced in Sections II-A and II-B, respectively. The total radiated power beampattern can be defined as the total received power P at each angle under investigation θ', and can be formally written as

$$P[\theta'] = \mathbb{E}\left[|r[n,\theta']|^2\right], \tag{12}$$

where θ' denotes the angle under investigation, t is the time instant and $\mathbb{E}$ is the statistical expectation operator.

A. Alternating Beamforming Case

The first considered system configuration is alternating the signals $S_1[n]$ and $S_2[n]$ in the antennas, as depicted in Fig. 2(a). Specifically, the even indexed antennas will transmit the beamformed signal $S_1[n]$ while the odd indexed signal $S_2[n]$. Therefore, following (10), the received signal at angle θ' can be written as

$$\begin{aligned} r_{\text{alt}}[n,\theta'] = {} & A[n]\exp(j\phi[n])\cdot \\ & \Bigg[\left(1+j\sqrt{\frac{1}{A[n]^2}-1}\right)\sum_{m\ \text{even}}\exp(j(a_{m,\theta'}-\psi_m))+ \\ & \left(1-j\sqrt{\frac{1}{A[n]^2}-1}\right)\sum_{m\ \text{odd}}\exp(j(a_{m,\theta'}-\psi_m))\Bigg]. \end{aligned} \tag{13}$$

Omitting the complete derivation, following (12), the beampattern expression can then be written as

$$\begin{aligned} P_{\text{alt}}[\theta'] = {} & \frac{4}{1-\cos(2\beta_{\theta'})} \\ & \times \Bigg[\cos(\beta_{\theta'})\left(1-\cos(M\beta_{\theta'})\right)\sigma_x^2 \\ & + \sin(\beta_{\theta'})\left(1-\cos(M\beta_{\theta'})\right) \\ & \times \left(-\frac{4}{3}\sqrt{\frac{\pi}{3}}\left(\sqrt{\sigma_x^2}\right)^3+\frac{1}{\sqrt{3}}\sigma_x^2+\frac{2}{3}\sqrt{\frac{\pi}{3}}\sqrt{\sigma_x^2}+\frac{1}{18\sqrt{3}}\right) \\ & + \frac{1}{2}\left(\cos(\beta_{\theta'})-1\right)\left(\cos(M\beta_{\theta'})-1\right)\Bigg] \end{aligned} \tag{14}$$

where $\sigma_x^2 = \mathbb{E}\left[A[n]^2\right]$ is the variance of the input signal $x[n]$. The angle under investigation θ' and the intended user angle θ are included within the coefficient $\beta_{\theta'}$ for the sake of brevity as

$$\beta_{\theta'} = 2\pi\rho(\sin(\theta') - \sin(\theta)). \tag{15}$$

Furthermore, the beampattern in (14) is dependent on $\mathbb{E}\left[A[n]\sqrt{1-A[n]^2}\right]$, which is approximated by using the third order Taylor series, at point 0.5.

It can be seen from (14) that the expression is ill-defined precisely at the intended angle, i.e., when $\theta' = \theta$. In this case, the expression will take the form of $0/0$. However, we can utilize the well-known L'Hôpital's rule to find the limit of the beampattern, as θ' approaches θ. By applying L'Hôpital's rule to (14), we get

$$\lim_{\theta' \to \theta} P_{\text{alt}}[\theta'] = M^2 \sigma_x^2, \tag{16}$$

indicating that the array gain is dependent only on the amount of employed antennas and the original transmit signal power.

B. Block Beamforming Case

In the second beamforming case, the signals $S_1[n]$ and $S_2[n]$ are grouped such that the first $M/2$ antennas transmit $S_1[n]$ and the latter $M/2$ antennas transmit $S_2[n]$. This scheme is illustrated in Fig. 2(b), and due to the sub-array type of structure of the feeding signals, may be easier to implement on hardware than the alternating scheme. Due to the changed signal configuration, the received signal in this case is written as

$$\begin{aligned} r_{\text{bl}}[n, \theta'] = \; & A[n] \exp(j\phi[n]) \cdot \\ & \Bigg[\left(1 + j \sqrt{\frac{1}{A[n]^2} - 1} \right) \sum_{m=0}^{\frac{M}{2}-1} \exp(j(a_{m,\theta'} - \psi_m)) + \\ & \left(1 - j \sqrt{\frac{1}{A[n]^2} - 1} \right) \sum_{m=\frac{M}{2}}^{M-1} \exp(j(a_{m,\theta'} - \psi_m)) \Bigg], \end{aligned} \tag{17}$$

and, following (12), the total power beampattern can be derived as

$$\begin{aligned} P_{\text{bl}}[\theta'] = & \frac{1}{1 - \cos(\beta_{\theta'})} \\ & \times \Bigg[\left(4\cos((M/2)\beta_{\theta'}) - 2\cos(M\beta_{\theta'}) - 2 \right) \sigma_x^2 \\ & + \left(4\sin((M/2)\beta_{\theta'}) - 2\cos(M\beta_{\theta'}) \right) \\ & \times \left(-\frac{4}{3}\sqrt{\frac{\pi}{3}} \left(\sqrt{\sigma_x^2} \right)^3 + \frac{1}{\sqrt{3}} \sigma_x^2 + \frac{2}{3}\sqrt{\frac{\pi}{3}} \sqrt{\sigma_x^2} + \frac{1}{18\sqrt{3}} \right) \\ & + 3 - 4\cos((M/2)\beta_{\theta'}) + \cos(M\beta_{\theta'}) \Bigg] \end{aligned} \tag{18}$$

which uses the same definition for $\beta_{\theta'}$ as shown in (15) and utilizes the same third order Taylor approximation for $\mathbb{E}\left[A[n]\sqrt{1 - A[n]^2}\right]$ as was used in (14). The beampattern in (18) is also ill-defined at $\theta' = \theta$, and we can again apply L'Hôpital's rule to obtain the limit at this point, which is given as

$$\lim_{\theta' \to \theta} P_{\text{bl}}[\theta'] = M^2 \sigma_x^2, \tag{19}$$

showing that the two presented cases have the same array gain at the intended angle.

IV. Simulation Results

In this Section, both of the beamforming schemes introduced in Section III are tested via simulations. We will compare the derived beampatterns of both cases from Section III to the simulated ones. Furthermore, we will study the proposed schemes compared to the more widely used Cartesian model. In a Cartesian transmitter architecture, the received signal can be simply written as

$$r_{\text{Cart}}[n, \theta'] = \sum_{m=0}^{M-1} \exp(j(a_{m,\theta'} - \psi_m)) x[n], \tag{20}$$

following the same reasoning as with the outphasing structure. It is then a simple matter to derive the beampattern for this case, which can be written as

$$P_{\text{Cart}}[\theta'] = \frac{1 - \cos(M\beta_{\theta'})}{1 - \cos(\beta_{\theta'})} \sigma_x^2, \tag{21}$$

again following the same reasoning as in the outphasing cases.

Additionally, we will simulate the inband and OOB emission levels at each angle θ' of the two outphasing beamforming cases and the Cartesian case. For a fair comparison of the three cases, we will adopt a PA model, through which the individual antenna signal are fed. Both the inband and OOB powers are evaluated through fast Fourier transform (FFT) of the far-field received signal at each direction, and the power is integrated over the inband and adjacent band portions of the FFT result. For the OOB emission level, the higher adjacent band power is chosen. Moreover, to further assess the capabilities of the considered beamforming schemes, commonly used metrics of EVM and TRP-based ACLR are evaluated with nonlinear PAs present. The EVM evaluates the inband signal quality at the intended receiver, and can be determined as

$$\text{EVM} = \sqrt{\frac{\sum_{k=1}^{K} |s_{\text{meas}}[k] - s[k]|^2}{\sum_{k=1}^{K} |s[k]|^2}} \times 100\ \%, \tag{22}$$

where $s_{\text{meas}}[k]$ is the kth measured (received) symbol, $s[k]$ the ideal transmit kth symbol and K the total amount of transmit symbols. The TRP-based ACLR on the other hand allows to quantify the OOB emissions taking into account the spatial characteristics of the radiated signals, which is key, as the power of the radiated distortion heavily depends on the considered angle. The TRP-based ACLR is defined as [4]

$$\text{TRP-ACLR} = 10\log_{10}\left(\frac{\sum_{\theta'} P_{\text{IB}}[\theta']}{\sum_{\theta'} P_{\text{OOB}}[\theta']} \right), \tag{23}$$

where $P_{\text{IB}}[\theta']$ is the inband power, and $P_{\text{OOB}}[\theta']$ the higher adjacent channel power. For FR-2 systems, 3GPP imposes a limit of 28 dB for the TRP-ACLR [10]. Lastly, the above metrics are further evaluated, when the individual antenna branches have mismatches in gain and in phase.

In the simulations, the following parametrization is adopted unless otherwise noted: $M = 32$, $\rho = 0.25$, $\sigma_x^2 = 0.156$, $\theta = -27°$. The variance σ_x^2 corresponds to a 5G NR compliant

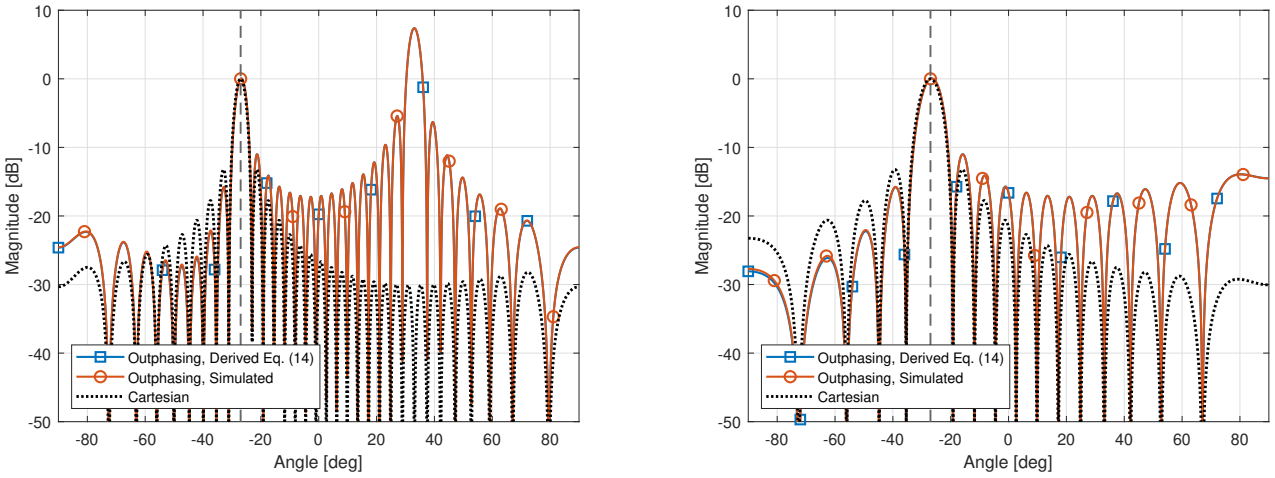

Fig. 3. The derived and simulated beampatterns utilizing the alternating beamforming scheme, with (a) $\rho = 0.5$ and (b) $\rho = 0.25$. The dashed vertical line indicates the intended angle $\theta = -27°$, ($M = 32$). The power is normalized to the power at the user angle.

200 MHz OFDM signal with 8 times oversampling, which is also utilized in the inband and OOB power simulations. The PAPR of the signal is limited through clipping and filtering, producing a PAPR of 8 dB and an EVM floor of about 1.9%. The utilized signals are 16-QAM modulated. For the purposes of this paper, we approximate the clipped and filtered OFDM signal as Gaussian distributed.

A. Beampattern with Alternating Beamforming

Let us first examine the beampattern of the alternating signal beamforming scheme. Due to the outphasing signals alternating in the antennas, it can be easily seen that the antenna separation needs to be halved compared to traditional Cartesian ULA approach, to avoid the generation of the grating lobes, since the effective antenna separation of two elements transmitting the same signal is now 2ρ. The grating lobes are created when the separation of antennas transmitting the same signal is greater than $\lambda/2$, as basic antenna theory reveals [18]. To see this effect, the derived and simulated beampatterns with $\rho = 0.5$ and $\rho = 0.25$ are illustrated in Fig. 3. It can be seen that the derived beampattern follows the simulated one very well, despite the utilized Taylor series approximation. It is also visible that with $\rho = 0.5$ the beampattern indeed exhibits a grating lobe. Mathematically, we can see this effect in Equation (14), as the antenna separation affects the period of the common denominator $2-2\cos(2\beta_{\theta'})$. The denominator will have two zeroes with $\rho = 0.5$, while having only one with $\rho = 0.25$, which then correspond to infinitely high peaks when taking the reciprocal.

The beam is also skewed slightly to the right of the intended angle, an effect which is caused by the sine terms in Equation (14). The odd sine functions have a zero at the intended angle, and consequently the values before and after the intended angle have different signs, which ultimately results in the beam pointing not precisely to the intended angle.

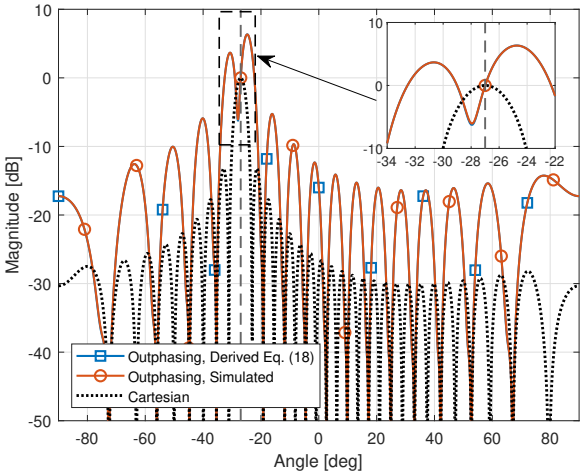

Fig. 4. The derived and simulated beampatterns utilizing the block beamforming scheme, with $\rho = 0.5$. The dashed vertical line indicates the intended angle $\theta = -27°$ ($M = 32$). The power is normalized to the power at the user angle.

B. Beampattern with Block Beamforming

The block beamforming scheme was presented as an alternative way to feed the outphasing signals to the antennas. We can see from Equation (18) that the block based solution does not introduce any additional grating lobes compared to the Cartesian one. This is due to the effective antenna separation being the same as in the Cartesian case. Therefore, the denominator $2 - 2\cos(\beta_{\theta'})$ has an identical structure to the Cartesian-based beampattern in Equation (21), where only

TABLE I
EVM AND TRP-BASED ACLR OF THE SCHEMES AT THE INTENDED USER ANGLE, WITH DIFFERENT AMOUNT OF TRANSMIT ANTENNAS. EVM FLOOR AT 1.9%

Metric	Antennas	Cartesian	Outphasing	
			Alternating	Block
EVM (%)	32	7.0	1.9	1.9
	128	7.0	1.9	1.9
	512	7.0	1.9	1.9
TRP-ACLR (dB)	32	30.5	21.9	13.1
	128	30.5	27.7	13.1
	512	30.5	34.1	13.1

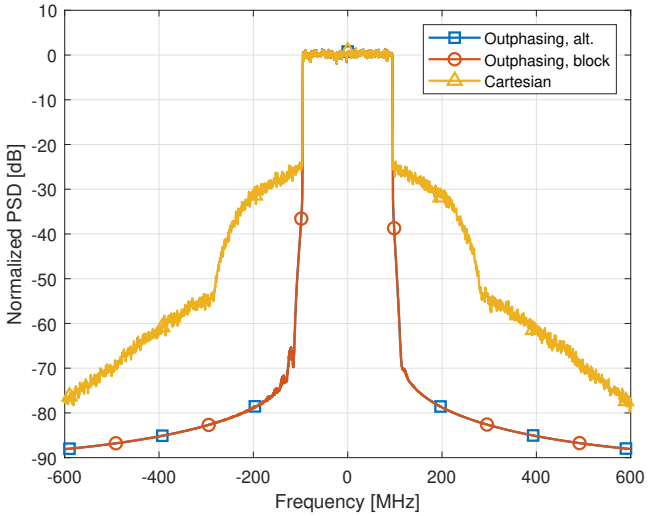

Fig. 5. PSDs of the received signals at the intended user angle, with amplification in nonlinear PAs. ($M = 32, \rho = 0.25$)

a single zero appears at the intended angle direction with $\rho = 0.5$.

Fig. 4 illustrates the derived and simulated beampatterns in the case of the block-based solution. The derived one follows the simulated one fairly well, the minor difference emerging simply from the use of the Taylor approximation also in this case. We can see that indeed, the issue of the grating lobes is eliminated by transmitting the signals in blocks, thus conserving the effective antenna separation from the basic Cartesian structure. However, the main beam in this case is visibly skewed to the right of the intended angle, much more so than in the alternating signals case. This effect stems again from the sine functions in the beampattern expression, which are now more powerful than in the alternating signal case. Therefore, we see a powerful beam just to the side of from the intended user angle.

C. Inband Distortion and OOB Emissions

In order to simulate the effects of the nonlinear PAs, the transmit signals have to be passed through PA models. For this, we utilize a memoryless modified Saleh model, which incorporates both the AM-AM and AM-PM responses for a PA, with parameters $\alpha_z = 0.82$, $\alpha_\phi = -0.35$, $\beta_z = 0.29$, $\beta_\phi = 1$ and $\epsilon = -0.36$ [19]. It is noted here that the outphasing component CE signals do not excite nonlinear behavior in the Saleh PA model, and it is used mainly for fair comparison between combinerless outphasing and Cartesian architecture OOB emissions.

Fig. 5 illustrates the power spectral densities (PSDs) of the received signals at the intended user angle, when utilizing the three different signaling schemes, after amplification in nonlinear PAs. It is clear that the nonlinear distortion of the PA affects the signal characteristics of the Cartesian case, by inducing strong spectral regrowth. Meanwhile, the outphasing-based schemes are visibly unaffected by the nonlinear distortion, and the signals combine perfectly to produce the original transmit signal. However, the component signals $S_1[n]$ and $S_2[n]$ are highly nonlinear separately, and do not combine coherently at angles excluding the intended angle, therefore Fig. 6 plots the inband and OOB powers of the different schemes at different angles. The plots are normalized to the inband power at the intended angle, which is the same for all the cases. The inband powers of the alternating case in Fig. 6(a) follow the Cartesian case fairly well, with the difference growing from around 1 dB near the intended angle to around 9 dB at angles near 60°. The block-based outphasing scheme suffers from the same slant near the intended angle as the total power beampattern, and the difference to the Cartesian case is larger than in the alternating case when moving away from the intended angle. On the other hand, the OOB powers in Fig. 6(b) show more difference between the cases. First, as was seen in Fig. 5, the OOB power at the intended angle is insignificant in the outphasing cases, whereas the Cartesian case demonstrates a high OOB power at this angle. However, the OOB power of the Cartesian case decreases when moving away from the intended angle, which is not the case in the alternating outphasing scheme, where the OOB power of the side lobes steadily rises from around -40 dB level to -30 dB at 60°. In the block-based approach, the OOB power also decreases further away form the intended angle, yet the powers are considerably higher than in the other two cases.

Table I shows the simulated EVM and TRP-based ACLR results for separate cases with 32, 128 and 512 antennas, averaged over 100 realizations. It is clear that the nonlinear distortion induced by the PA affects the EVM in the Cartesian case, where clipping of the signal occurs within the PA, while the EVM is invariable when utilizing the outphasing schemes, due to the CE component signals. The amount of utilized transmitter antennas has no effect on the perceived EVM, as the values stay constant even with 512 antennas. The TRP-based ACLR is above the 28 dB limit with Cartesian signaling, whereas both of the outphasing cases demonstrate TRP-ACLR values well below the limit when employing 32 antennas. However, increasing the transmitting antennas has the effect of improving the TRP-ACLR in the alternating outphasing case, a level of 34.1 dB can be achieved with 512 antennas. However, there is no discernible effect on the other two cases

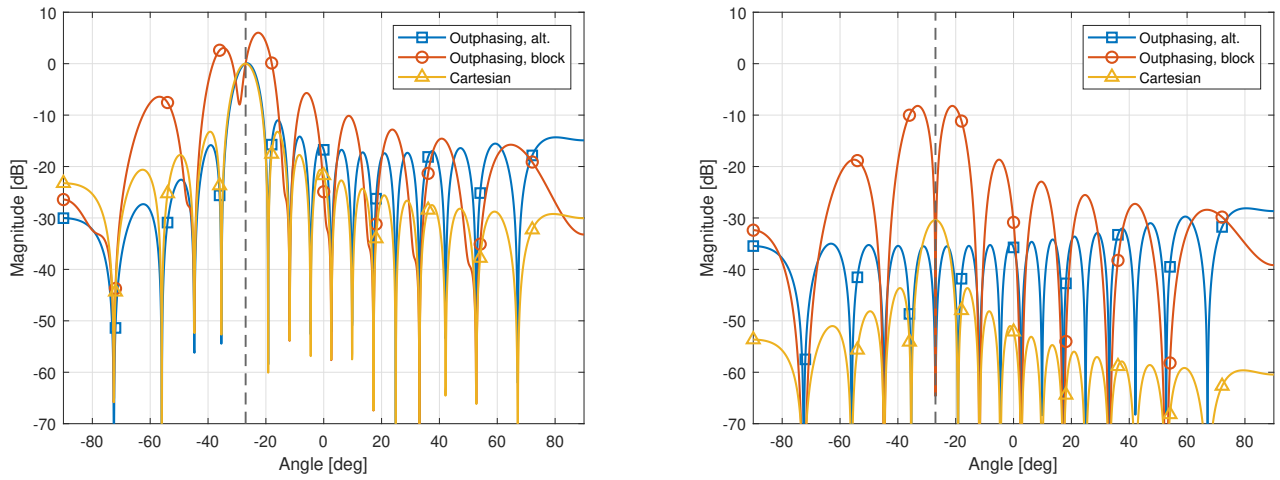

Fig. 6. Inband (a) and OOB (b) powers at each direction with the transmit signals amplified in nonlinear PAs, with the two considered outphasing and Cartesian transmitters ($M = 32, \rho = 0.25$). The power is normalized to the inband power at the user angle.

with varying amount of antennas. Based on these results and taking into account also the total power beampatterns, it seems that the alternating outphasing structure is favorable over the block-based approach.

D. Antenna Branch Gain and Phase Mismatch

So far, we have considered the transmitter system and channel ideal, the only imperfections stemming from the nonlinear PAs used in the previous subsection. Here, we additionally consider the effects of the mismatches in gain and phase in the antenna branches, in terms of the signal quality metrics of EVM and TRP-ACLR. The model of the individual antenna signal $\hat{y}_m[n]$ at branch indexed m under gain and phase mismatch is given, following (8), as

$$\hat{y}_m[n] = \exp(j(R_{m,p} - \psi_m)S_{1,2}[n](1 + R_{m,g}) \qquad (24)$$

where $R_{m,g}$ and $R_{m,p}$ are Gaussian distributed random variables with zero mean and standard deviation of σ_r. The signals $\hat{y}_m[n]$ will then be amplified in the nonlinear PAs, transmitted and combined at the receiver as described in Section II. The signals under the mismatches are simulated for different amounts of antennas, ranging from 32 to 512. Additionally, three different standard deviations for the mismatches are considered, ranging from 0.01 to 0.1. The EVM at the intended angle θ and TRP-ACLR results are averages of 100 realizations, and are seen in Fig. 7.

From Fig. 7 it is discernible that the mismatches have a negative effect on the EVM performance in all of the systems, yet employing more antennas makes the outphasing structures perform much closer to the EVM floor, whereas the Cartesian structure's performance is unaffected by the number of antennas. The same is true for the Cartesian architecture in the TRP-ACLR case, where the performance is invariable in terms of the number of antennas. This also holds for the block-based outphasing structure, where the TRP-ACLR is well below the 28 dB limit. On the other hand, in the alternating outphasing signaling case the TRP-ACLR performance improves with increasing number of antennas. In this case, the 28 dB limit is reachable with sufficiently many antennas, depending on the severity of the mismatches in the antenna branches.

V. Conclusion

In this paper, we have considered two distinct cases for the outphasing transmitter where the combining of the signals occurs OTA, in an antenna array context, as a potential, more efficient, substitute for the widely-used Cartesian architecture. We derived the mathematical expressions for the total power beampatterns in these cases, which show that the patterns differ slightly from the basic Cartesian one. Signal quality considerations through the EVM showed the benefit of the outphasing scheme under highly nonlinear PAs. However, the TRP-based ACLR limit of 28 dB imposed by 3GPP could not be met without substantially increasing the amount of transmitter antennas. The results suggest that the alternating outphasing scheme is superior to the block-based solution in terms of radiation patterns. Additionally, the reported results indicate that while the combinerless outphasing has potential, it still needs further investigation and innovations to be a completely feasible substitute for the widely-used Cartesian architecture.

Acknowledgement

This work was supported in part by the Academy of Finland under Grants 323461, 321613, and 301820.

References

[1] C. Fager *et al.*, "Linearity and Efficiency in 5G Transmitters: New Techniques for Analyzing Efficiency, Linearity, and Linearization in a 5G Active Antenna Transmitter Context," *IEEE Microw. Mag.*, vol. 20, no. 5, pp. 35–49, May 2019.

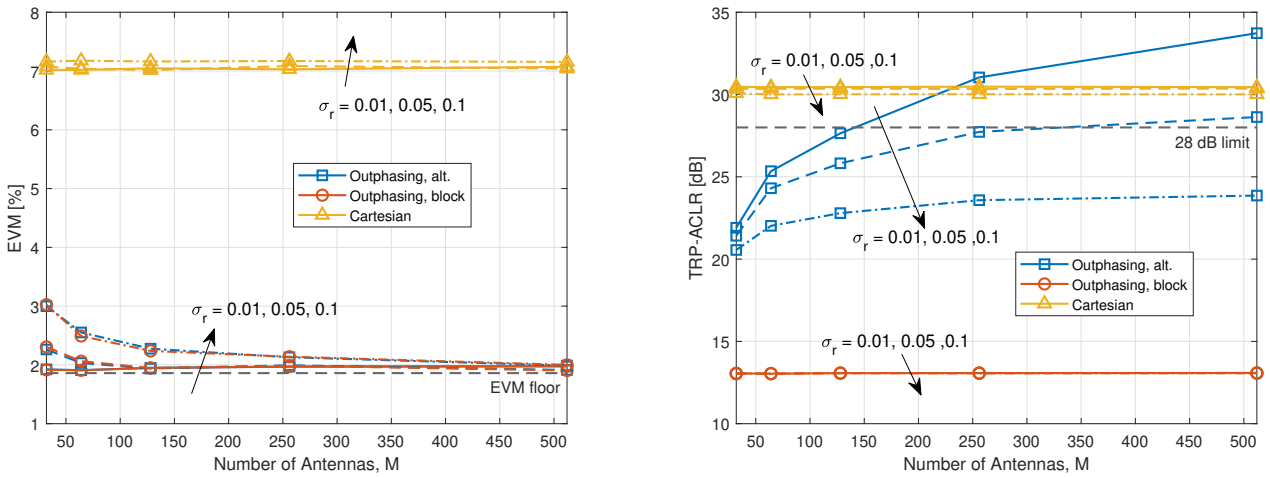

Fig. 7. EVM (a) and TRP-ACLR (b) results with various number of employed antennas and standard deviations of the mismatches, after amplification in nonlinear PAs, utilizing the two considered outphasing and Cartesian transmitters (ρ= 0.25).

[2] A. Li, C. Masouros, F. Liu, and A. L. Swindlehurst, "Massive MIMO 1-bit DAC Transmission: A Low-complexity Symbol Scaling Approach," *IEEE Trans. Wireless Commun.*, vol. 17, no. 11, pp. 7559–7575, Nov. 2018.

[3] X. Liu *et al.*, "Beam-oriented Digital Predistortion for 5G Massive MIMO Hybrid Beamforming Transmitters," *IEEE Trans. Microw. Theory Techn.*, vol. 66, no. 7, pp. 3419–3432, Jul. 2018.

[4] A. Brihuega *et al.*, "Piecewise Digital Predistortion for mmWave Active Antenna Arrays: Algorithms and Measurements," *IEEE Trans. Microw. Theory Techn.*, vol. 68, no. 9, pp. 4000–4017, Sep. 2020.

[5] S. K. Mohammed and E. G. Larsson, "Per-antenna Constant Envelope Precoding for Large Multi-user MIMO Systems," *IEEE Trans. Commun.*, vol. 61, no. 3, pp. 1059–1071, Mar. 2013.

[6] S. Zhang, R. Zhang, and T. J. Lim, "Constant Envelope Precoding for MIMO Systems," *IEEE Trans. Commun.*, vol. 66, no. 1, pp. 149–162, Jan. 2018.

[7] H. Chireix, "High Power Outphasing Modulation," *Proc. IRE*, vol. 23, no. 11, pp. 1370–1392, Nov. 1935.

[8] D. Cox, "Linear Amplification with Nonlinear Components," *IEEE Trans. Commun.*, vol. 22, no. 12, pp. 1942–1945, Dec. 1974.

[9] T. Barton, "Not Just a Phase: Outphasing Power Amplifiers," *IEEE Microwave Magazine*, vol. 17, no. 2, pp. 18–31, 2016.

[10] 3GPP Tech. Spec. 38.104, "NR; Base Station (BS) radio transmission and reception," *v15.9.0, (Release 15)*, April 2020.

[11] S. Ali, B. Adebisi, G. Markarian, and E. Arikan, "Signal Combining in LINC Amplifier Using Alamouti Codes," *Electron. Lett.*, vol. 46, no. 18, pp. 1301–1302, Sep. 2010.

[12] C. Liang and B. Razavi, "Transmitter Linearization by Beamforming," *IEEE J. Solid-State Circuits*, vol. 46, no. 9, pp. 1956–1969, Sep. 2011.

[13] W.-R. Wu, S.-L. Cheng, and Y.-P. Hsu, "Maximum Likelihood Detection for Coded Combinerless LINC-OFDM Systems," *EURASIP J. Wirel. Commun. and Netw.*, no. 153, pp. 1–14, Jun. 2016.

[14] E. J. Martínez-Pérez *et al.*, "T-LINC Architecture with Digital Combination and Mismatch Correction in the Receiver," in *Proc. IEEE NORCAS*, Helsinki, Finland, Oct. 29-30, 2019, pp. 1–5.

[15] B. G. M. van Ark, A. B. Smolders, and P. F. M. Smulders, "Outspacing Phased Arrays for mm-Wave 5G Base Stations," in *Proc. 14th EuCAP*, Copenhagen, Denmark, Mar. 15-20, 2020, pp. 1–5.

[16] P. N. Landin, J. Fritzin, W. Van Moer, M. Isaksson, and A. Alvandpour, "Modeling and Digital Predistortion of Class-D Outphasing RF Power Amplifiers," *IEEE Trans. Microw. Theory Tech.*, vol. 60, no. 6, pp. 1907–1915, Jun. 2012.

[17] A. Birafane *et al.*, "Analyzing LINC Systems," *IEEE Microw. Mag.*, vol. 11, no. 5, pp. 59–71, Aug. 2010.

[18] C. A. Balanis, *Antenna theory: analysis and design*. John wiley & sons, 2016.

[19] M. O'droma, S. Meza, and Y. Lei, "New Modified Saleh Models for Memoryless Nonlinear Power Amplifier Behavioural Modelling," *IEEE Communications Letters*, vol. 13, no. 6, pp. 399–401, 2009.